*energies*

MDPI

*Article*

# Optimal Scheduling Model of a Battery Energy Storage System in the Unit Commitment Problem Using Special Ordered Set

**Insu Do and Siyoung Lee ***

Department of Energy & Electrical Engineering, Tech University of Korea (TUK), Siheung 15073, Korea; dis9406@tukorea.ac.kr

* Correspondence: slee0519@tukorea.ac.kr; Tel.: +82-31-8041-0697

**Abstract:** Nonlinear characteristics of a battery energy storage system (BESS) may cause errors in the stored energy between the operation plan and the actual operation. These errors may hinder the reliability of the power system especially in environments such as microgrids with limited power generation resources and high uncertainty. This study proposes a method to alleviate the occurrence of such errors in the charging/discharging scheduling process of the BESS by piecewise linearizing its nonlinear characteristics. Specifically, the stored energy in a BESS that changes nonlinearly according to the size of the charging/discharging power was modeled using the special ordered set of the type 2 (SOS2) method. The proposed model and the typical BESS-operation models with constant power conditioning system (PCS) input/output power efficiency were applied to the unit commitment (UC) problem in a microgrid environment, and the results were compared with the actual operation results. The proposed model operated similarly to the actual operation compared to the typical model, reducing the error in charging/discharging energy. Consequently, the proposed model was made cost-effective by reducing the cost of error correction and reduced the risk of deviating from operating range of the BESS. This study demonstrates that the proposed method can efficiently solve the operational problems caused by the nonlinear characteristics of BESS.

**Keywords:** battery energy storage system (BESS); microgrid; mixed-integer linear programming (MILP); piecewise linearization; special ordered set of type 2 (SOS2)



**Citation:** Do, I.; Lee, S. Optimal Scheduling Model of a Battery Energy Storage System in the Unit Commitment Problem Using Special Ordered Set. *Energies* **2022**, *15*, 3079. https://doi.org/10.3390/en15093079

Academic Editors: Yun-Su Kim, Jin-Oh Lee and Djaffar Ould-Abdeslam

Received: 22 March 2022
Accepted: 20 April 2022
Published: 22 April 2022



## 1. Introduction

BESSs have been used as useful power sources over the years. With the increase in renewable energy generation, BESS is being discussed more actively from an operational point-of-view regarding the reliability and economy of the grid. BESSs are being utilized as major resources, especially in small-scale microgrids, wherein resources are limited and require more accurate operational scheduling. Because the microgrid is associated with a small load and comprises a small number of generators, it may be more sensitive to changes in the renewable energy output or system faults [1]. In addition, if it is connected to the main grid, the risk associated with the case in which no power is received (owing to an external problem) should be considered. For these reasons, BESSs in microgrids have become more important than those in large power systems.

Various studies have reported on the use of BESSs in microgrids. In [2], BESS was presented as one of the means for reducing the peak load. BESS charges during the off-peak time period, and discharges during the peak-time period to reduce the peak load. BESS has also been studied as a way to stabilize the system risk from intermittent renewable energy generation [3]. In addition, various previous studies exist on this topic, such as a study which presented a method by which to control the frequency and voltage fluctuations of a microgrid using a BESS [4,5].

Previous studies focused on the purpose of using a BESS in a microgrid situation, in which the proportion of BESS resources is large. Most of these previous studies assumed

that the mathematical model of the BESS itself was a simple linear model that could be used to reduce the complexity of the operation. However, this simple model cannot accurately reflect the losses that occur nonlinearly in the actual BESS charging/discharging process. As a result, when the charge/discharge schedule of the BESS derived from the optimization model is implemented, an error occurs pertaining to the stored energy in the BESS. This error can lead to situations in which actual physical operation is impossible in microgrids with limited available resources.

To solve this problem, previous studies that focused on the nonlinear characteristics of the charging/discharging efficiency of the BESS are examined in this study. These studies and their findings are applied to the charging/discharging scheduling problem of BESS. Specifically, the mathematical optimization model of the BESS is elaborated on by linearizing the input/output power curve of the BESS PCS by using SOS2 and by reflecting the loss in the idle state.

## 2. Previous Studies

Studies of various mathematical models have been conducted to reflect the physical characteristics of BESS charging/discharging in scheduling problems. First, the stored energy $soe_t$ in the battery is calculated as follows:

$$soe_t = E_t^{tf} + E_t^{ch} - E_t^{dis} \tag{1}$$

At this time, the stored energy $soe_t$ in the battery is calculated by the relation between the transferred energy from the previous time $E_t^{tf}$ and the charging and discharging energies at the present time $E_t^{ch}$ and $E_t^{dis}$, respectively. Several methods have been studied for the calculation of $E_t^{tf}$, $E_t^{ch}$, and $E_t^{dis}$.

A method exists for the calculation of the relationship between the charging/discharging energies and the stored energy through efficiency [6]. The efficiency of the BESS should also be considered when applying the BESS with generators to the system. The amount of energy charged/discharged in the system differs from the amount of energy stored in the battery, which can be expressed in the form of efficiency. The efficiency of a BESS is typically divided into the following three categories: rate of self-discharge $\gamma^s$ over time, charging efficiency $\gamma^{ch}$, and discharging efficiency $\gamma^{dis}$. These are typically expressed by their application to the constraints of the stored energy in a battery [7]. Accordingly, the following equation can be used:

$$soe_t = \gamma^s \, soe_{t-1} + \gamma^{ch} \, P_t{}^{ch} P_t{}^{dis} / \gamma^{dis} \tag{2}$$

The current stored energy in the battery $soe_t$ is expressed by the relation between the previously stored energy $soe_{t-1}$, the charging power $P_t{}^{ch}$, and the discharging power $P_t{}^{dis}$. When applying the above equation as a constraint for the BESS, there are various approaches to choose from to determine the efficiency.

The most basic method involves the application of constant values to efficiency during all scheduling periods. The most frequently used method among them is the case in which only the charging efficiency $\gamma^{ch}$ is considered as the turn-around efficiency without considering the rate of self-discharge of battery $\gamma^s$ and discharging efficiency $\gamma^{dis}$ [2,8,9]. In the case of [10–13], a constant value was used to consider the charging efficiency $\gamma^{ch}$ and discharging efficiency $\gamma^{dis}$ during the scheduling period. This method is the simplest and can be applied because there are no additional constraints on efficiency during the scheduling period. In addition, this method has the advantage of being able to express battery storage characteristics without significantly increasing the complexity of the simulation, as it only requires a few simple linear constraints to solve complex UC problems. However, applying a constant efficiency for all periods is disadvantageous owing to the large difference from actual operation scenarios because the realistic characteristics of the battery cannot be properly applied. Because the efficiency is calculated as a constant, even

if the same energy is charged and discharged, an error occurs in battery energy storage during actual operation that may cause problems in optimized scheduling management.

Meanwhile, previous studies have reported the physical characteristics based on which the charging/discharging rates decrease according to the stored energy [14]. In [14], a method was presented to add the physical properties of the storage state to the equation for energy storage.

$$soe_t = \gamma^s \cdot soe_{t-1} + \gamma^{ch} \cdot P_t^{ch'} - P_t^{dis} / \gamma^{dis} \tag{3}$$

$$P_t^{ch'} \leq P_t^{ch} \tag{4}$$

$$P_t^{ch'} \leq P_t^{ch} \cdot \frac{E^{cap} - soe_t}{E^{cap} - soe^{CC,CV}} \tag{5}$$

Equation (3) applies a linear change in the charging energy according to the battery storage state, in addition to the existing constant efficiency. That is, this equation represents the physical characteristics of the battery for which the charging rate slows down as the charging state approaches 100%. In Equation (5), $E^{cap}$ represents the energy capacity of the BESS, and $soe^{CC,CV}$ is the stored energy state of the battery used as a reference for changes in the battery's charging rate. In Equation (3), $P_t^{ch'}$ denotes the value to which the aforementioned constraints are applied to according to Equation (2). Equation (4) indicates that maximum charging is possible in all energy storage states. In cases in which the battery storage state is $soe^{CC,CV}$ or higher, the charging energy gradually decreases as the stored energy increases according to Equation (5). The charging rate in the model linearly decreases from $P_t^{ch}$ (when $soe_t = soe^{CC,CV}$) to zero (when $soe_t = E^{cap}$). However, in this model, only one other physical characteristic was added when the battery capacity exceeded a certain value. In addition, with the exception of the applied physical characteristics, the charging/discharging efficiency used a constant efficiency so that the model might differ from the actual operation.

Previous studies were represented by a linear model. However, the physical characteristics of the actual BESSs are nonlinear, and some studies reflect these nonlinear characteristics. The case in which the efficiency of nonlinearity was considered can be confirmed in [15]. The efficiency function of a BESS consists of a sum of the following three parts: storage state $soe_t$, $F_t^{ch}$ and $F_t^{dis}$. Among them, $F_t^{ch}$ and $F_t^{dis}$ are expressed as functions with temperature $T$, $P_t^{ch}$, $P_t^{dis}$ and as variables. If the function is used, a more accurate result can be obtained than when compared to that of a linearly approximated model. This is because a more accurate efficiency calculation is possible in the low-efficiency interval. The basic equation is expressed as follows:

$$soe_t = \gamma^s \cdot soe_{t-1} + F_t^{ch}\left(P_t^{ch}, soe_{t-1}, T\right) - F_t^{dis}\left(P_t^{dis}, soe_{t-1}, T\right) \tag{6}$$

However, dynamic programming was used to find the optimal solution of nonlinear Equation (6) in [15]. Therefore, the method of [15] has the problem that it is difficult to apply the proposed ESS model to other MIP-based scheduling optimization problems such as UC.

## 3. Modeling

This section describes the process used to mathematically model the nonlinear characteristics of a BESS and these characteristics are applied to a mixed integer linear programming (MILP)-based UC model. First, an SOS2 model, which is a mathematical method used for the piecewise linearization of a nonlinear function, is described. A method that applies the SOS2 model to the nonlinear characteristics of the BESS is then proposed. The last part of this section examines how the BESS model, linearized based on the proposed SOS2, is used in the UC problem in conjunction with other power generation sources.

### 3.1. Special Ordered Set of Type 2

In the problem of power system scheduling, piecewise linearization is generally applied to the objective function [16]. In this case, the linearization function is convex; thus, it can be applied. Therefore, in this study, the SOS2 method was used to perform piecewise linearization in a nonconvex function, such as the efficiency of the BESS. The SOS2 method can proceed with linearization with a small number of variables and constraints, and has the advantage of being numerically stable in the linearization process [17].

SOS2 is a general linearization method for nonlinear functions and is used to convert nonlinear optimization problems into MILP forms. The value of the point at which the slope change occurs is the change point, and SOS2 proceeds with piecewise linearization as the sum of the weights of the change points at both ends of each interval. Figure 1 depicts the process of expressing the piecewise linearization function $f$ of the nonlinear function $F$ using the SOS2 method. As shown in Figure 1, the variable $X$, which exists in the interval $u_i$, can be calculated by using the near change points $x_i$ and $x_{i+1}$ of the interval $u_i$ and their weights $w_i$ and $w_{i+1}$. Because $f$ is linear in each interval, it can also be expressed as a linear sum of the weights $w_i$ and $w_{i+1}$, as shown in Figure 1. This SOS2 process is expressed by Equations (7)–(11) as follows [18]:

$$X = \sum_{i=1}^{I} (w_i \cdot x_i) \tag{7}$$

$$\sum_{i=1}^{I} w_i = 1, \ (w_i \geq 0) \tag{8}$$

$$f(X) = \sum_{i=1}^{I} (w_i \cdot F(x_i)) \tag{9}$$

$$\sum_{i=1}^{K} u_i = 1, \ (u_i = 0 \text{ or } 1) \tag{10}$$

$$w_i \leq u_{i-1} + u_i, \ (u_0 = u_I = 0) \tag{11}$$

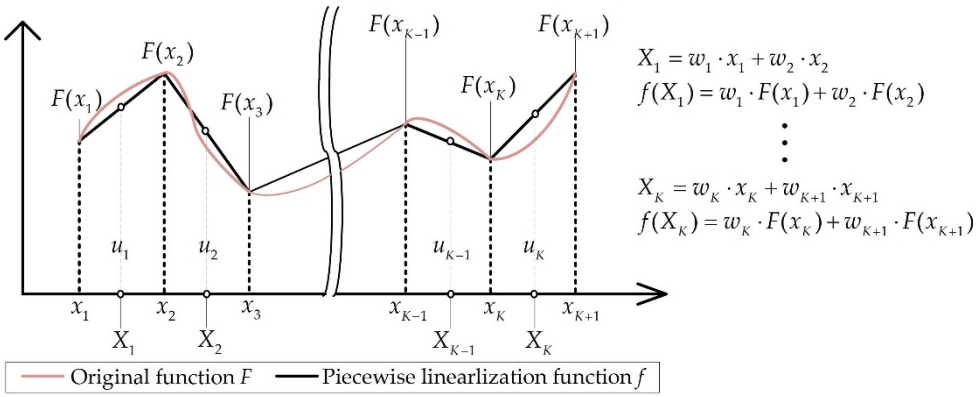


**Figure 1.** Example of SOS2 application to function $F$.

First, if the number of divided intervals is set to $K$, the number $I$ of the change points whose slope changes, as shown in Figure 1, is set to $K + 1$. In Equations (7) and (8), the variable $X$ is calculated using the data $x_i$ and weight $w_i$ of each change point, as shown in Figure 1. $w_i$ calculated using Equations (7) and (8) is applied to $F(x_i)$, substituting each change point $x_i$, as shown in Figure 1, in Equation (9) to calculate $F(X)$. Equations (10) and (11) are constraints that only allow two change points to be used at both ends of the interval where $X$ exists. The binary variable $u_i$ is 1 if $X$ exists within the interval. Equation (10) allows for only one interval to be selected, and Equation (11) allows for only $w_i$ at both ends of the selected interval to be used.

### 3.2. BESS Operation Constraint

As described in Section 2, three efficiency values $\gamma^s$, $\gamma^{ch}$, and $\gamma^{dis}$ must be considered to calculate the current stored energy of battery $soe_t$ over time in accordance with the charging/discharging powers ${P_t}^{ch}$ and ${P_t}^{dis}$. In this study, the value of $\gamma^s$ was constant and was focused on modeling the nonlinearities of $\gamma^{ch}$ and $\gamma^{dis}$. The nonlinearities of $\gamma^{ch}$ and $\gamma^{dis}$ are mainly caused by the PCS battery characteristics. Figure 2 shows the PCS efficiency curves of BESS as introduced in other studies [19–22].

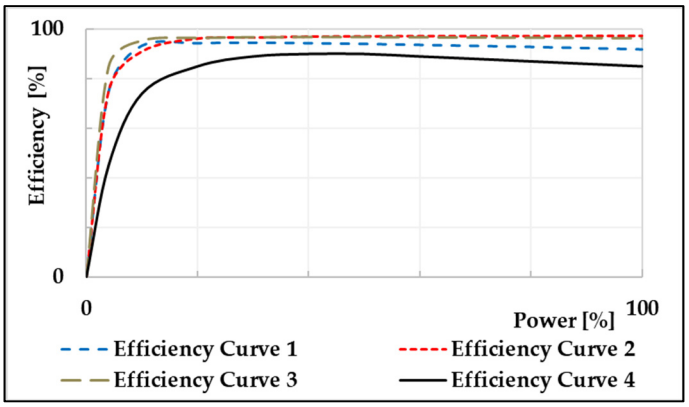


**Figure 2.** Typical Efficiency curves from [19–22].

As illustrated in Figure 2, it is common to have small values in low-power intervals and relatively high values in high-power intervals. In this paper, to express the nonlinear characteristics of $\gamma^{ch}$ and $\gamma^{dis}$, the mathematical model proposed in [23] and based on the converter efficiency curve was modified and used as follows:

$$\gamma_t^{ch/dis} = G_t(P_t^{ch/dis}) = \frac{1}{\frac{a}{P_t^{ch/dis}} + b \cdot P_t^{ch/dis} + c} \tag{12}$$

In conclusion, this research considered only changes in efficiency depending on the input/output power changes during charging/discharging, with the exception of nonlinearities depending on external factors, such as temperature $T$ and $soe$ changes.

The method used to calculate the stored energy $soe_t$ by applying the function $G$ to Equation (2) can be expressed according to Equation (13).

$$soe_t = \gamma^s \cdot soe_{t-1} + {P_t}^{ch} \cdot G_t({P_t}^{ch}) - {P_t}^{dis} / G_t({P_t}^{dis}) \tag{13}$$

In this case, an appropriate linearization process is required to apply the nonlinear characteristics of the BESS to the MILP-based UC model in Equation (13). However, if the function $G$ is piecewise linearized based on the application of the SOS2 examined in Equation (13), $E_t^{ch}$ includes the quadratic term of ${P_t}^{ch}$, and $E_t^{dis}$ includes the variable according to ${P_t}^{dis}$ in the denominator term. As a result, $soe_t$ becomes a nonlinear constraint expressed by a fractional equation containing the quadratic terms of ${P_t}^{ch}$ and ${P_t}^{dis}$. To solve this nonlinearity problem, this study applied SOS2 to the charging/discharging energies $E_t^{ch}$ and $E_t^{dis}$ expressed as $P_t^{ch} \cdot G(P_t^{ch})$ and $P_t^{dis} \cdot G(P_t^{dis})$, respectively, rather than in terms of the function $G$ in Equation (13). Figure 3 shows the nonlinear functions ${F_t}^{ch}$ and ${F_t}^{dis}$ of charging/discharging energies $E_t^{ch}$ and $E_t^{dis}$, which change according to the charging/discharging powers ${P_t}^{ch}$ and ${P_t}^{dis}$, respectively.

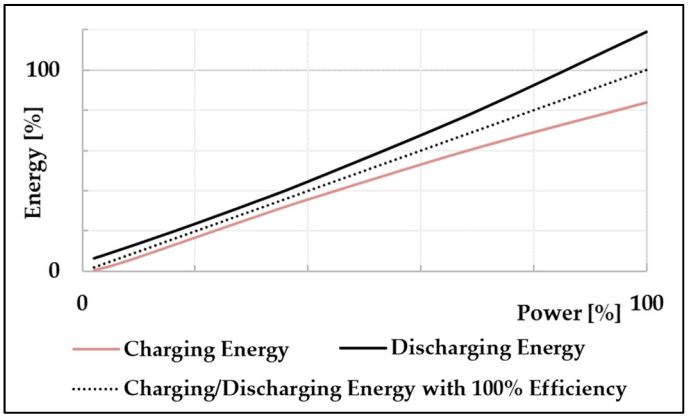


**Figure 3.** Charging/discharging energies based on function ${F_t}^{ch}$ and ${F_t}^{dis}$.

To apply Equations (7)–(11) of SOS2 presented in Section 3.2 to the BESS, the variable $X$, nonlinear function $F$, and change point $x_i$ shown in Figure 1, need to be changed to charging/discharging power ${P_t}^{ch}/{P_t}^{dis}$, charging/discharging energy function ${F_t}^{ch}/{F_t}^{dis}$, and change point ${P_t}^{point}$. The other linearization processes are the same as those represented by Equations (7)–(11). Finally, the linearization notation for the charging energy function ${F_t}^{ch}$ is as follows:

$$P_t^{ch} = \sum_{i=1}^{I} (w_{i,t} \cdot P_i^{point}) \tag{14}$$

$$\sum_{i=1}^{I} w_{i,t} = 1, (w_i \geq 0) \tag{15}$$

$$f_t^{ch}(P_t^{ch}) = \sum_{i=1}^{k} (w_{i,t} \cdot F_t^{ch}(P_i^{point})) \tag{16}$$

$$\sum_{i=1}^{K} u_{i,t}^{interval} = 1, \ (u_t^{interval} = 0 \text{ or } 1) \tag{17}$$

$$w_{i,t} \leq u_{i-1,t}^{interval} + u_{i,t}^{interval}, \ (u_{0,t}^{interval} = u_{I,t}^{interval} = 0) \tag{18}$$

The discharging energy function ${F_t}^{dis}$ can be linearly expressed as the same as the charging energy function ${F_t}^{ch}$, as in Equations (14)–(18).

### *3.3. Unit Commitment*

In this study, the constraints of commonly used UC models were used. The objective function of the UC model was to minimize the operating costs of the system. For operating costs, the cost of the hourly power generation $P_{g,t}$ of each generator alongside the fuel cost $C^{fuel}$ and the start-up cost $C^{start-up}$ of the generators were considered together, as shown in Equation (19). Herein, $u_{g,t}^{start}$ is a binary variable used to denote the instant at which the generator begins to operate.

$$\min \sum_{t \in T, g \in G} P_{g,t} C_g^{fuel} + C_g^{start-up} u_{g,t}^{start} \tag{19}$$

The following Equations (20)–(33) are constraints of the UC model used.

$$D_t - P_t^{ren} = P_{g,t} + P_t^{ch} - P_t^{dis} \tag{20}$$

$$P_g^{\min} \cdot u_{g,t}^{onoff} \leq P_{g,t} \leq P_g^{\max} \cdot u_{g,t}^{onoff} \tag{21}$$

$$P_{g,t-1} - P_{g,t} \leq RD_g \tag{22}$$

$$P_{g,t} - P_{g,t-1} \leq RU_g \tag{23}$$

$$u_{g,t}^{onoff} - u_{g,t-1}^{onoff} = u_{g,t}^{start} - u_{g,t}^{stop} \tag{24}$$

$$u_{g,t}^{start} + u_{g,t}^{stop} \leq 1 \tag{25}$$

$$u_{g,t}^{start} + \sum_{k=t+1}^{t+MU_g} u_{g,k}^{stop} \leq 1 \tag{26}$$

$$u_{g,t}^{stop} + \sum_{k=t+1}^{t+MD_g} u_{g,k}^{start} \leq 1 \tag{27}$$

Equation (20) indicates that the power supplied at all times and the demand $D$ must match. This model considers renewable energy and a BESS. Therefore, the generated power $P_{g,t}$, renewable power generation $P_t^{ren}$, and the charging/discharging powers of BESS ${P_t}^{ch}$ and ${P_t}^{dis}$ supplied per hour in Equation (20) are also considered.

Equations (21)–(27) are the constraints of the generator's characteristics. The maximum and minimum generation limits of each unit are imposed in Equation (21). $P_g^{\max}$ and $P_g^{\min}$ are the maximum and minimum output of each generator, respectively. The binary variable $u_{g,t}^{onoff}$ indicates the operating state of the generator. Equations (22) and (23) are the constraints of the ramp up/down rates. The constraints are restricted by the use of the difference in the power generation amount between timepoints $t$ and $t+1$, and $RU_g$ and $RD_g$ are the maximum output amounts that can be ramped up or down for each generator. Equations (24)–(27) impose the minimum up and down times for each unit, respectively. Both $u_{g,t}^{start}$ and $u_{g,t}^{stop}$ are binary variables of the starting-up and shutting-down signals of each generator, respectively. In Equations (26) and (27), $MU_g$ and $MD_g$ means minimum up and down time each generator.

$$E^{cap} \cdot soe^{\min} \leq soe_t \leq E^{cap} \cdot soe^{\max} \tag{28}$$

$$soe_0 = E^{cap} \cdot soe^{init} \tag{29}$$

$$soe_{fin} = E^{cap} \cdot soe^{fin} \tag{30}$$

$$P_t^{ch} \leq P^{ch,\max} \cdot u_t^{ch} \tag{31}$$

$$P_t^{dis} \leq P^{dis,\max} \cdot u_t^{dis} \tag{32}$$

$$u_t^{ch} + u_t^{dis} \leq 1 \tag{33}$$

Equations (28)–(33) are constraints in cases in which the BESS is applied to the UC model. Equation (28) constrains the energy storage of the BESS to operate within a specific range, i.e., it is defined for values greater or equal to $soe^{\min}$ (%), and values less or equal to $soe^{\max}$ (%). Equations (29) and (30) constrain the initial and final conditions of the energy storage using $soe^{init}$(%) and $soe^{fin}$(%), respectively. Equations (31)–(33) constrain the charging/discharging power $P^{ch,\max}$ and $P^{dis,\max}$ by using the operational status binary variables $u_t^{ch}$ and $u_t^{dis}$. The charging and discharging energies from the BESS is then calculated using Equations (13)–(18), based on the SOS2 method. As an additional constraint, $soe_t$ is calculated using Equation (13) presented in Section 3.2. In addition, to calculate $soe_t$, the charging energy $E_t^{ch}$ represented by the nonlinear function ${F_t}^{ch}$ and the discharging energy $E_t^{dis}$ represented by the nonlinear function ${F_t}^{dis}$ are calculated using Equations (14)–(18) based on SOS2.

## 4. Case Study

### *4.1. Scenario Data*

To verify the effect of the proposed BESS-operation method, the following two BESS modeling methods were applied to the same microgrid system to obtain the results.

- Method I: assume that $\gamma^s$, $\gamma^{ch}$, and $\gamma^{dis}$ are constant
- Method II: proposed method using SOS2

In addition, Method I was subdivided into two methods according to the values of $\gamma^{ch}$ and $\gamma^{dis}$ to analyze diverse situations.

- Method $I_{70}$: $\gamma^{ch}$,$\gamma^{dis}$ = 70%
- Method $I_{80}$: $\gamma^{ch}$,$\gamma^{dis}$ = 80%

The microgrid for effectiveness verification consists of four diesel generators, solar and wind power plants, and one BESS. The characteristics of the four generators and BESS were obtained using data from a previous study [10]. Table 1 shows the characteristics of the generators of the microgrid, and Table 2 lists the BESS characteristics for performing Method I.

**Table 1.** Characteristics of thermal units.

| Generator | Unit Cost [$/MWh] | Min–Max Capacity [MW] | Min Up/Down Time [h] | Ramp Up/Down Rate [MW/h] | Start-Up Cost [$] |
|---|---|---|---|---|---|
| G1 | 27.7 | 2–10 | 3 | 4 | 50 |
| G2 | 39.1 | 1–5 | 3 | 3 | 20 |
| G3 | 61.3 | 1–5 | 3 | 3 | 20 |
| G4 | 65.6 | 0.8–3 | 1 | 2.5 | 5 |

**Table 2.** Characteristics of BESS.

| BESS | Capacity [MWh] | Charging/ Discharging Max Power [MW] | $soe_t$ Operation Range [%] | Initial, Final Target $soe_t$ [%] | Charging/ Discharging Efficiency [%] | Rate of Self-Discharge [%] |
|---|---|---|---|---|---|---|
| | 5 | 5 | 10–90 | 50 | 70, 80 | 99 |

Method II uses the same characteristics as the BESS used in Method I, but $\gamma^{ch}$ and $\gamma^{dis}$ are calculated and applied using the change points listed in Table 3.

**Table 3.** Change points of PCS efficiency curve.

| Change Point | Point 1 $\gamma_{c,d}$ = 0% | Point 2 30.92% | Point 3 54.16% | Point 4 71.78% | Point 5 79.99% | Point 6 84.42% | Point 7 88.43% | Point 8 89.60% | Point 9 87.89% | Point 10 84.07% |
|---|---|---|---|---|---|---|---|---|---|---|
| $P_t^{ch,dis}$ [MW] | 0 | 0.1 | 0.25 | 0.5 | 0.75 | 1 | 1.5 | 2 | 3.5 | 5 |
| $F_t^{ch}(P_t^{ch})$ [MWh] | 0 | 0.031 | 0.135 | 0.359 | 0.600 | 0.844 | 1.326 | 1.792 | 3.076 | 4.204 |
| $F_t^{dis}(P_t^{dis})$ [MWh] | 0 | 0.323 | 0.462 | 0.697 | 0.938 | 1.185 | 1.696 | 2.232 | 3.982 | 5.947 |

The efficiency value of the change points in Table 3 was obtained from [22], as shown in Figure 2. Based on this data set, the coefficients $a$, $b$, and $c$ of the nonlinear function $G$ introduced in Equation (12) were derived as 0.2326, 0.0477, and 0.9042 through curve fitting. This fitted function $G$ is plotted in Figure 4. To present the characteristics of the function $G$ assumed more efficiently above, the change point sets the interval more closely in the low-output interval with a large change in value. At this time, as mentioned in Section 3.2, the change point applies the nonlinear functions $F_t^{ch}$ and $F_t^{dis}$ as shown in Figure 3, and not $\gamma^{ch}$ or $\gamma^{dis}$, to eliminate the nonlinearity problem.

In addition, scenarios of load and renewable-energy generation patterns were diversified to determine the effects of the proposed change in method II depending on the microgrid system status. In other words, to show various patterns, the actual load of PJM Regional Transmission Organization (RTO) [24] in 2019 was scaled to match the microgrid environment, wherein solar and wind power were assumed to be generated. The data created are shown in Figure 5.

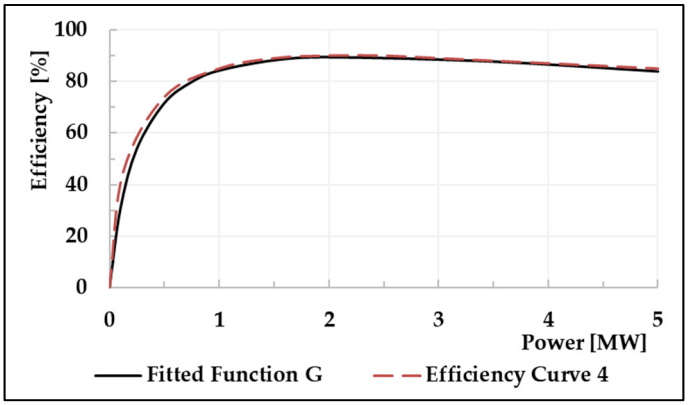


**Figure 4.** Fitted function *G* based on the value of change points in Table 3.

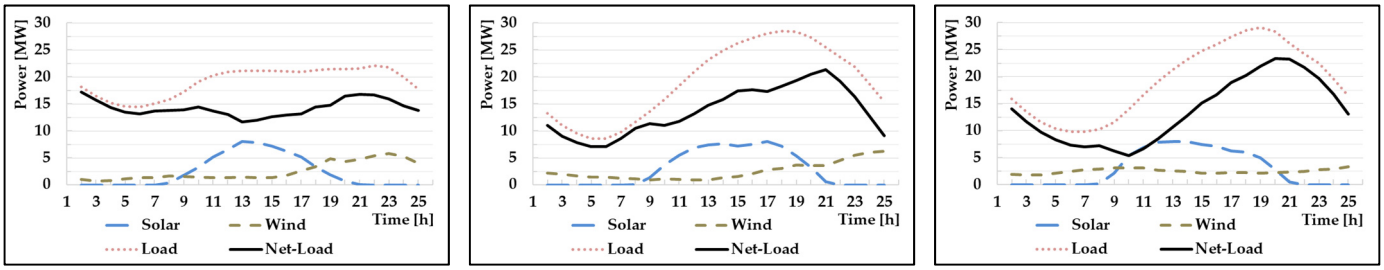


**Figure 5.** Load and renewable energy generation patterns for scenarios (**a**) A, (**b**) B, and (**c**) C.

Scenarios for each of the three data patterns on which the simulation was performed were labeled A to C, sequentially. Scenario A is a pattern that is generally observed in the spring of the PJM, and the load factor is high because of the small difference between the peaks and off-peak instants. In addition, scenarios B and C have load patterns similar to patterns observed in the summer, but exhibit differences in net load patterns owing to differences in renewable energy generation. Accordingly, the case may be displayed. For example, the codename "Case I–A" indicates that methods I and A are used to load data. In the experiments, all case simulations were performed daily, and the length of each time period was set to 1 h.

Based on the above data, all experiments were performed on an Intel Core 3.70 GHz processor with 16 GB random access memory using Xpress-MP [25], which is a general-purpose MIP solver.

### *4.2. Results*

In this section, the results of each scenario were analyzed and verified by comparing them with the results obtained when nonlinearity was applied. The charging/discharging energy of the BESS calculated based on Methods I and II for each scenario yielded an error with the actual value calculated based on function *G*. This error increased the uncertainty regarding the energy available for power supply and the suppliable period. When the BESS is operated in an actual power system to solve this problem, a separate mechanism is required to correct the error between the planned and the actual $soe_t$ schedules. The error correction mechanism leads to additional BESS operation costs. However, because a clear answer to the error-correction mechanism has not yet been presented, it is difficult to quantify the costs. Therefore, in this study, it was assumed that this error correction mechanism was not specified, and costs were consumed at a certain unit price to correct the stored energy error for each time period that occurred in the BESS. The assumed error correction unit price was determined to be \$70/MWh considering the operating cost of the G4 power source, which could be operated and stopped freely in the microgrid presented

in Section 4.1. The overall cost and BESS operating pattern for each case calculated in this way can be found in Table 4 and Figures 6–11, respectively.

**Table 4.** Overall cost and maximum Error in $soe_t$ comparison of the three methods presented herein during one day.

| | Scenarios | Method $I_{70}$ | Method $I_{80}$ | Method II |
|---|---|---|---|---|
| A | Overall cost | 100.7 | 100.5 | 100.0 |
| | Error correction costs | 0.262 | 0.300 | 0.005 |
| | Maximum error of $soe_t$ [MWh] | 0.332 | 0.322 | 0.008 |
| B | Overall cost | 102.2 | 101.9 | 101.1 |
| | Error correction costs | 0.431 | 0.526 | 0.019 |
| | Maximum error of $soe_t$ [MWh] | 0.587 | 0.322 | 0.026 |
| C | Overall cost | 106.7 | 106.3 | 105.2 |
| | Error correction costs | 0.913 | 0.830 | 0.006 |
| | Maximum error of $soe_t$ [MWh] | 0.548 | 0.509 | 0.008 |

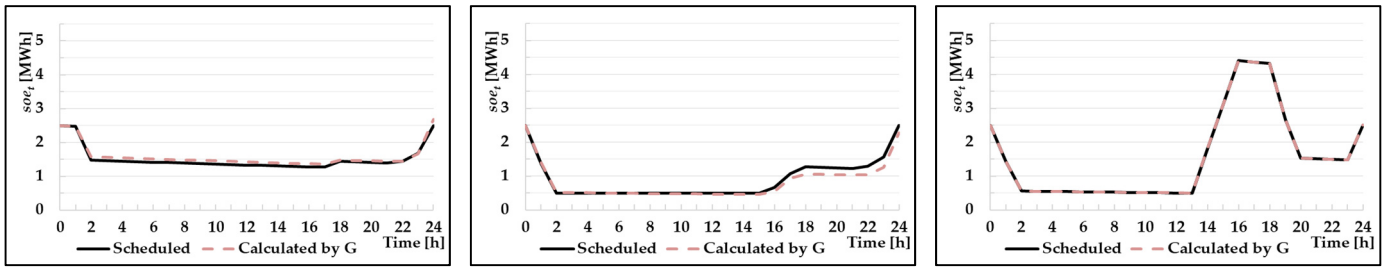


(**a**) (**b**) (**c**)

**Figure 6.** Variations of $soe_t$ for Scenario A using methods (**a**) $I_{70}$, (**b**) $I_{80}$, and (**c**) II.

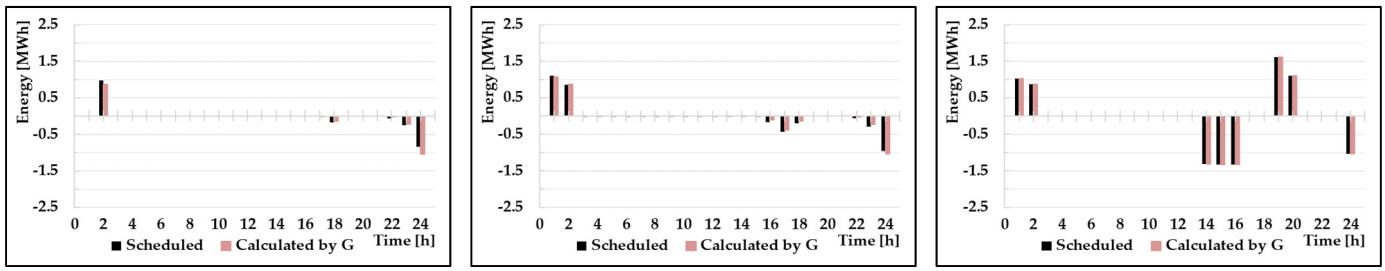


(**a**) (**b**) (**c**)

**Figure 7.** Charging/discharging patterns for Scenario A using methods (**a**) $I_{70}$, (**b**) $I_{80}$, and (**c**) II.

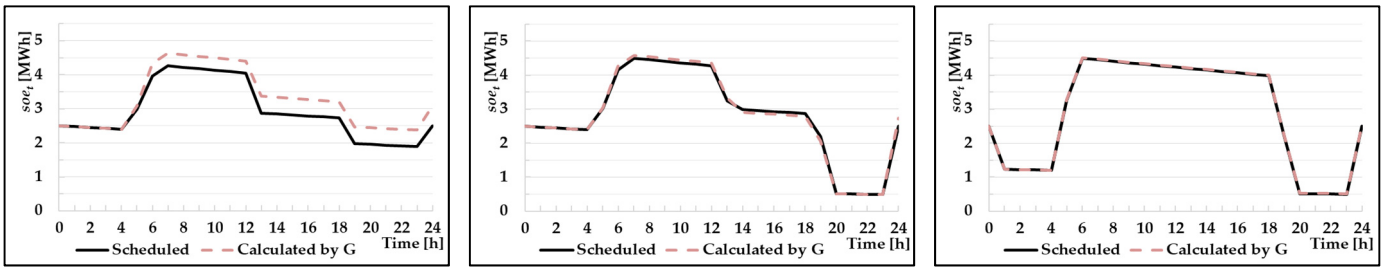


(**a**) (**b**) (**c**)

**Figure 8.** Variations of $soe_t$ for Scenario B using methods (**a**) $I_{70}$, (**b**) $I_{80}$, and (**c**) II.

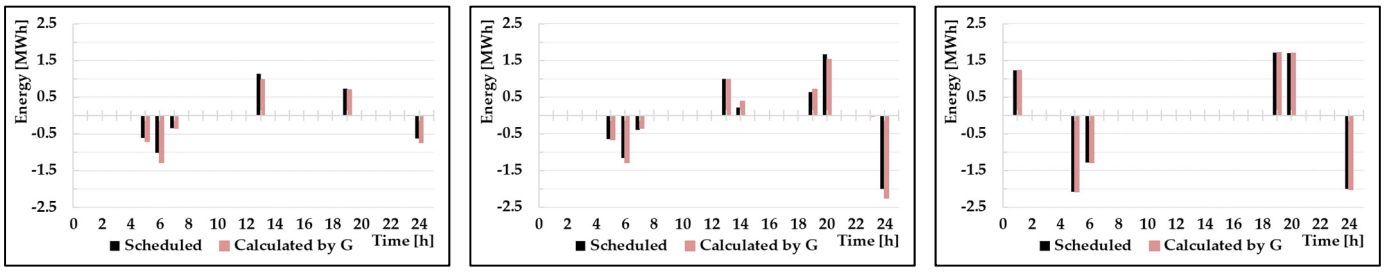


(**a**) (**b**) (**c**)

**Figure 9.** Charging/discharging patterns for Scenario B using methods (**a**) $I_{70}$, (**b**) $I_{80}$, and (**c**) II.

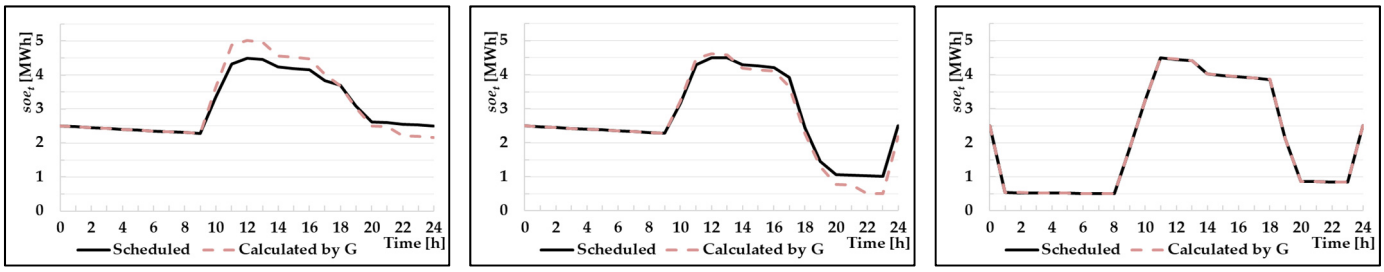


(**a**) (**b**) (**c**)

**Figure 10.** Variations in $soe_t$ for Scenario C using methods (**a**) $I_{70}$, (**b**) $I_{80}$, and (**c**) II.

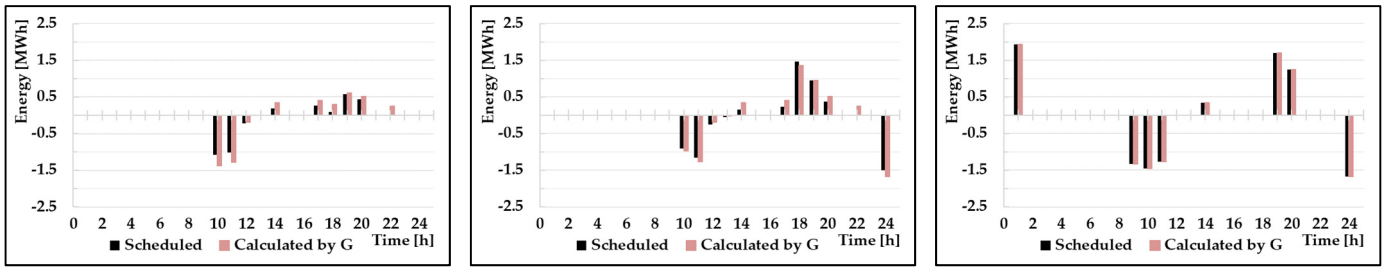


(**a**) (**b**) (**c**)

**Figure 11.** Charging/discharging patterns for Scenario C using methods (**a**) $I_{70}$, (**b**) $I_{80}$, and (**c**) II.

The overall costs listed in Table 4 include error correction costs in the total generator operating costs during the scheduling period. The error correction cost was calculated based on considerations of the accumulated error between the error correction unit price (approximately \$70/MWh) defined earlier and the actual energy storage calculated by function *G*. All the costs were scaled to 100, based on changing the overall cost of Case II–A (\$10,844.5), which had the lowest overall cost during the scenario period. Based on scenarios A, B, and C, the overall cost and error correction costs of Methods I and II gradually increased. Method II had the lowest cost. The cause for this can be identified through the BESS operation pattern. Figures 6–11 show the BESS operation pattern scheduled for Methods I and II, and the BESS operation pattern calculated by function *G*.

Figure 6 illustrates that compared with Case $I_{80}$–A, which uses 80% constant efficiency, the $soe_t$ result of Case $I_{70}$–A is similar to the result obtained when the actual nonlinear function is applied.

However, as shown in Table 4, Case $I_{80}$–A did not generate a considerable error in $soe_t$ compared to the other cases. This is because the load factor (82.8%) of the net load in Scenario A was high, which resulted in poor BESS utilization. In particular, in this situation, the frequency of charging and discharging of the BESS decreased in the cases of methods $I_{70}$ and $I_{80}$ at a low, constant efficiency; thus, the actual result value and accumulated energy error decreased. Conversely, Case II–A, in which method II was used, had a higher BESS utilization than Case I–A. This is because the BESS operates in a high-efficiency output interval by assessing the charging and discharging energy, as shown in Figure 7.

Case $I_{80}$–B is similar to the actual value of $soe_t$ compared with the value obtained in Case $I_{70}$–B. This is attributed to the fact that the actual average charge power of Case $I_{80}$–B was approximately 0.71 MW and the discharge power was approximately 1.05 MW. When this value is substituted in function *G*, the efficiencies are approximately equal to 79% and 85%. These values are close to 80%. Accordingly, it can be observed that even if a constant efficiency is applied, a value that is similar to the actual result can be obtained. However, in Case $I_{70}$–B, the operating range at 06:00 a.m. is approximately 3% outside of the upper limit of the operating range. This is because the actual charging/discharging-energy efficiency according to the charging/discharging power was 70% or more. The $soe_t$ shown in Figure 8, is outside the upper operating range because the actual charging energy increases during charging and the energy used during discharging decreases. The actual charging/discharging energy is shown in Figure 9. This means that the optimal constant efficiency varies depending on the system status. In addition, it can be observed that the utilization of BESS increased compared with Scenario A which is presented in Figure 6.

In Scenario C, both Cases $I_{70}$–C and $I_{80}$–C, in which method I was used, were outside the specified operating range. Because the efficiencies of 70% and 80% applied to Method I are intermediate values of the nonlinear efficiency curve, errors may occur in both the upper and lower limits of the $soe_t$ operating range depending on the charging and discharging powers. In Scenario C, the actual $soe_t$ result of Method $I_{70}$ in Figure 10 deviates from 5 MWh (BESS capacity) at 11:00 a.m. In addition, approximately 2.17 MWh is stored at the last point; this value is approximately 13% smaller than the 2.5 MWh of Method $I_{70}$. Case $I_{80}$–C also shows that errors can occur in both the upper and lower limits at 11:00 a.m. and 10:00 p.m. As shown in Figures 6–11, Scenario B has a higher utilization of BESS compared with Scenario A. In addition, in terms of cost, there are many energy errors accumulated at the same error correction unit price, thus resulting in an increase in the error correction cost. In addition, Scenario C yielded a BESS utilization profile similar to Scenario B, but the error correction cost increased because of the high BESS utilization in the low-power interval, which was associated with a high level of error in energy storage.

Even if Method I is applied, the result may be similar to the actual value based on function *G* if the constant efficiency is properly set according to the system environment. However, it is virtually impossible to change the efficiency of BESS scheduling in real time depending on the system environment. Therefore, an error occurs in the energy charged and discharged from the BESS, and as a result, this problem increases the possibility of $soe_t$ being outside the predetermined operating range. This may affect the reliability of a microgrid environment with a small number of thermal units. In addition, in terms of cost, as the utilization of BESS increases, the error-correction cost increases. Moreover, it can be observed that the error correction cost increases according to the charging/discharging power even within a similar utilization range. This shows the inefficiency and inaccuracy of Method I. However, in Figures 6–11, in all scenarios, Method II ensures a constant high level of accuracy, and is the most advantageous in terms of cost. This means that it can be applied regardless of the system status, and shows the high efficiency and usefulness of the proposed Method II.

## 5. Conclusions

This study proposed a method to reflect the nonlinear characteristics of the BESS charging/discharging efficiency during its operation. To achieve this, an optimization model was established in which the nonlinearity of the PCS efficiency was linearized by applying the SOS2 technique to the change in the charging/discharging energy. To verify the effectiveness of the proposed method, it was compared with a BESS operation model with a constant efficiency. For these comparisons, PJM data were selected on specific days and scaled according to a microgrid environment to establish a daily microgrid operation scenario. Each BESS operation model was applied to the generated scenarios to perform a daily UC, and the derived daily microgrid operation results were analyzed by focusing on operating costs and BESS charging/discharging patterns.

From the simulation results, the proposed method was confirmed to reduce the error between the planned and actual BESS schedule compared with the constant-efficiency method. In particular, the proposed method maintained the BESS operation error at a relatively small and constant level irrespective of the scenario, whereas the conventional method with constant efficiency yielded considerable variations in the BESS operation error depending on the scenario. In other words, the proposed method can reduce the uncertainty of BESS operation and is effective in terms of system operation cost, including the BESS error correction costs. Finally, to implement the actual system of the proposed method, future work needs to consider the error correction cost mechanism of the BESS operation error.

**Author Contributions:** Formal analysis, investigation, writing—original draft preparation, I.D.; conceptualization, methodology, writing—review and editing, S.L. All authors have read and agreed to the published version of the manuscript.

**Funding:** This research was funded by Korea Electric Power Corporation (Grant number: R21FT10) and Korea Institute of Energy Technology Evaluation and Planning (Grant number: 20193710100061).

**Institutional Review Board Statement:** Not applicable.

**Informed Consent Statement:** Not applicable.

**Data Availability Statement:** Not applicable.

**Conflicts of Interest:** The authors declare no conflict of interest.

## References

1. Etxeberria, A.; Vechiu, I.; Camblong, H.; Vinassa, J.M.; Camblong, H. Hybrid Energy Storage Systems for renewable Energy Sources Integration in microgrids: A review. In Proceedings of the International Power Engineering Conference (IPEC), Singapore, 27–29 October 2010.
2. Lobato, E.; Sigrist, L.; Rouco, L. Use of energy storage systems for peak shaving in the Spanish Canary Islands. In Proceedings of the IEEE Power & Energy Society General Meeting, Vancouver, BC, Canada, 21–25 July 2013.
3. Li, Y.; Yang, Z.; Li, G.; Zhao, D.; Tian, W. Optimal Scheduling of an Isolated Microgrid with Battery Storage Considering Load and Renewable Generation Uncertainties. *IEEE Trans. Ind. Electron.* **2019**, *66*, 1565–1575. [CrossRef]
4. Chowdhury, A.H.; Asaduz-Zaman, M. Load frequency control of multi-microgrid using energy storage system. In Proceedings of the 8th International Conference on Electrical and Computer Engineering, Dhaka, Bangladesh, 20–22 December 2014.
5. Lee, Y.D.; Jiang, J.L.; Su, H.J.; Ho, Y.H.; Chang, Y.R. Ancillary voltage control for a distribution feeder by using energy storage system in microgrid. In Proceedings of the 2016 IEEE 7th International Symposium on Power Electronics for Distributed Generation Systems (PEDG), Vancouver, BC, Canada, 27–30 June 2016.
6. Faisal, M.; Hanan, M.A.; Ker, P.J.; Hussain, A.; Mansor, M.B.; Blaabjerg, F. Review of Energy Storage System Technologies in Microgrid Applications: Issues and Challenges. *IEEE Access* **2018**, *6*, 35143–35164. [CrossRef]
7. Parisio, A.; Glielmo, L. A mixed integer linear formulation for microgrid economic scheduling. In Proceedings of the 2011 IEEE International Conference on Smart Grid Communications (SmartGridComm), Brussels, Belgium, 17–20 October 2011.
8. Byrne, R.H.; Silva-Monroy, C.A. Potential revenue from electrical energy storage in ERCOT: The impact of location and recent trends. In Proceedings of the 2015 IEEE Power & Energy Society General Meeting, Denver, CO, USA, 26–30 July 2015.
9. Senjyu, T.; Miyagi, T.; Yousuf, S.A.; Urasaki, N.; Funabashi, T. A technique for unit commitment with energy storage system. *Electr. Power Energy Syst.* **2007**, *29*, 91–98. [CrossRef]
10. Lee, J.H.; Lee, S.Y.; Lee, K.S. Multistage Stochastic Optimization for Microgrid Operation Under Islanding Uncertainty. *IEEE Trans. Smart Grid* **2021**, *12*, 56–66. [CrossRef]
11. Gholami, A.; Shekari, T.; Aminifar, F.; Shahidehpour, M. Microgrid Scheduling with Uncertainty: The Quest for Resilience. *IEEE Trans. Smart Grid* **2016**, *7*, 2849–2858. [CrossRef]
12. Chen, C.; Duan, S.; Cai, T.; Liu, B.; Hu, G. Optimal Allocation and Economic Analysis of Energy Storage System in Microgrids. *IEEE Trans. Power Electron.* **2011**, *26*, 2762–2773. [CrossRef]
13. Fossati, J.P.; Galarza, A.; Martín-Villate, A.; Echeverría, J.M.; Fontán, L. Optimal scheduling of a microgrid with a fuzzy logic controlled. *Electr. Power Energy Syst.* **2015**, *68*, 61–70. [CrossRef]
14. Pandzic, H.; Bobanac, V. An Accurate Charging Model of Battery Energy Storage. *IEEE Trans. Power Syst.* **2019**, *34*, 1416–1426. [CrossRef]
15. Nguyen, T.A.; Byrne, R.H.; Chalamala, B.R.; Gyuk, I. Maximizing the Revenue of Energy Storage Systems in Market Areas Considering Nonlinear Storage Efficiencies. In Proceedings of the 2018 International Symposium on Power Electronics, Electrical Drives, Automation and Motion (SPEEDAM), Amalfi, Italy, 20–22 June 2018.

16. Coffrin, C.; Knueven, B.; Holzer, J.; Vuffray, M. The impacts of convex piecewise linear cost formulations on AC optimal power flow. *Electr. Power Syst. Res.* **2021**, *199*, 107191. [CrossRef]
17. De Farias, I.R., Jr.; Zhao, M.; Zhao, H. A special ordered set approach for optimizing a discontinuous separable piecewise linear function. *Oper. Res. Lett.* **2008**, *36*, 234–238. [CrossRef]
18. Guéret, C.; Prins, C.; Sevaux, M. *Applications of Optimization with Xpress-MP*; Eyrolles: Paris, France, 2000; pp. 40–42.
19. Kersic, M.; Bocklish, T.; Bottiger, M.; Gerlach, L. Coordination Mechanism for PV Battery Systems with Local Optimizing Energy Management. *Energies* **2020**, *11*, 469. [CrossRef]
20. Bragard, M.; Soltau, N.; Doncker, R.W.D. Design and implementation of a 5 kW photovoltaic system with li-ion battery and additional DC-DC converter. In Proceedings of the 2010 IEEE Energy Conversion Congress and Exposition, Atlanta, GA, USA, 12–16 September 2010.
21. Arnieri, E.; Boccia, L.; Amoroso, F.; Amendola, G.; Cappuccino, G. Improved Efficiency Management Strategy for Battery-Based Energy Storage Systems. *Electronics* **2019**, *8*, 1459. [CrossRef]
22. KKoo, W.; Kim, D.H. Improved Operation Algorithm for Parallel Three Phase PWN Converter at Light Load Conditions. In Proceedings of the 2015 18th International Conference on Electrical Machines and Systems (ICEMS), Pattaya City, Thailand, 25–28 October 2015.
23. Vorpérian, V. Simple Efficiency Formula for Regulated DC-to-DC Converters. *IEEE Trans. Aerosp. Electron.* **2010**, *46*, 2123–2131. [CrossRef]
24. System Operation Data. Available online: https://dataminer2.pjm.com/list (accessed on 1 October 2021).
25. FICOXpress Optimization. 2020. Available online: https://www.fico.com/ (accessed on 1 October 2021).